Capon DOD/DOA Estimation Algorithm for Bistatic MIMO Radar Using Dipole Antenna Arrays with Known Mutual Coupling

Ouarda Barkat

University of Frères Mentouri – Constantine 1, Constantine, Algeria

https://doi.org/10.26636/jtit.2025.3.2121

Abstract — This study focuses on the joint estimation of the direction of departure (DOD) and direction of arrival (DOA) of multiple targets in bistatic multiple input multiple output (MIMO) radar systems employing orthogonal waveforms. A linear array of half-wavelength dipole antennas (HWD) with known mutual coupling is utilized. The proposed method applies a two-dimensional Capon (2D Capon) algorithm to estimate both the DOD and DOA of multiple targets. To mitigate the adverse effects of mutual coupling, an efficient compensation mechanism is integrated into the Capon direction-finding algorithm. This mechanism relies on realistic electromagnetic modeling in which mutual coupling is represented using Toeplitz-structured coupling matrices. Through computer simulations, the influence of various system parameters on the algorithms performance is evaluated, with particular emphasis on its resolution capability and estimation accuracy. The results clearly demonstrate that incorporating mutual coupling compensation significantly enhances the accuracy of the 2D Capon algorithm.

Keywords — bistatic MIMO radar, Capon method, DOD/DOA estimation, mutual coupling

1. Introduction

The concept of multiple input, multiple output (MIMO) has been widely used in the field of wireless communications in recent years [1]. Implementing this concept in radar systems allows the design of a virtual network larger than that of traditional systems [2]–[4]. These systems greatly enhance detection performance and robustness, improving target localization depending on the type of MIMO radar. The emergence of bistatic MIMO radars has further increased interest in estimating both the direction of departure (DOD) and the direction of arrival (DOA) [5]–[7].

The operating principle of bistatic MIMO radar, consisting of an array of half-wavelength dipole (HWD) antennas, is to dynamically create a beam pattern. This beam pattern is designed to have its main lobe directed toward the desired signal, enhancing detection and localization.

Consequently, various angle estimation algorithms have been developed for MIMO radars, including estimation of signal parameters via rotational invariance techniques (ESPRIT), multiple signal classification (MUSIC), and Capon algorithms.

Generally, the MUSIC algorithm is regarded as having higher estimation accuracy than the Capon algorithm. However, in MIMO radar applications, it is often observed that the Capon algorithm outperforms the MUSIC algorithm [8]–[11]. The two-dimensional Capon (2D Capon) algorithm is a well-established and effective technique for estimating both DOD and DOA in bistatic MIMO radar systems [12]–[14].

Although the algorithm itself is not new, its integration with a mutual coupling compensation strategy in a bistatic MIMO configuration constitutes a novel and valuable contribution.

In practical radar systems, mutual coupling between the elements of the array can significantly degrade performance, especially in the estimation of DOD and DOA, by introducing signal distortions that complicate the estimation process [15]–[18].

This work advances the state of the art by applying compensation techniques within the Capon framework and conducting a quantitative analysis of mutual coupling effects using realistic antenna models, such as HWD arrays.

The proposed approach offers medium to high potential impact in the radar signal processing community, as it improves the practical deployment of MIMO radar systems and enables a more robust angle estimation performance.

This paper focuses on the estimation of DOD and DOA in bistatic MIMO radar systems using the 2D Capon algorithm. However, it is well established that the 2D Capon algorithm is highly sensitive to mutual coupling between HWD antennas in the array. To evaluate the impact of mutual coupling, we used a simplified model of the HWD array. Leveraging extensive data on dipoles, we analyze an array of equidistantly spaced dipoles.

Simulation results demonstrate that the performance of the Capon algorithm deteriorates due to mutual coupling, with the degradation becoming more pronounced as the interelement spacing between antennas decreases. This performance degradation can be significantly mitigated by employing a compensating matrix that optimally adjusts the DOD and DOA estimates.

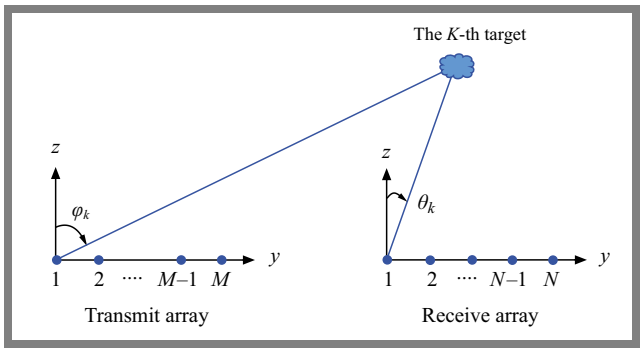

Fig. 1. Bistatic MIMO radar system.

2. The Theoretical Model

Figure 1 illustrates a bistatic MIMO radar system with K non-coherent targets. The transmitting array consists of M uniformly spaced half-wavelength antennas arranged along the y-axis with an inter-element spacing of d. Similarly, the receiving array consists of N HWD antennas, also arranged linearly, with the same spacing d between adjacent elements [19]–[21]. Each transmitting antenna emits an orthogonal signal $s_i(t)$ which is sampled every T seconds to obtain L snapshots.

In a bistatic radar system, the signals received on the receiving array after reflection from the K targets can be expressed as follows [18]:

$$X(t) = \sum_{i=1}^{K} (\beta_i \cdot \mathbf{c}_r(\varphi_i) \cdot \mathbf{a}_r(\varphi_i)) \cdot \left(\mathbf{c}_t(\theta_i) \cdot \mathbf{a}_t^T(\theta_i)\right) \cdot S(t) + Z(t) , \tag{1}$$

where: β_i is the complex amplitude of the i-th target, K is the total number of targets illuminated by the MIMO radar, φ_i and θ_i represent the DOD and DOA of the i-th target, respectively.

Typically, multiple samples are used to estimate (φ_i, θ_i), $i = 1, \ldots, K$, and the corresponding signal model with multiple snapshots L can be written as:

$$\mathbf{X}(L) = \sum_{i=1}^{K} \left(\beta_i \cdot \mathbf{c}_r(\varphi_i) \cdot \mathbf{a}_r(\varphi_i) \cdot \mathbf{c}_t(\theta_i) \cdot \mathbf{a}_t^T(\theta_i)\right) \cdot \mathbf{S}(L) + \mathbf{Z}(L) , \tag{2}$$

where:

- $\mathbf{Z}(L)$ represents the sensor noise, assumed to be non-uniform and modeled as a zero-mean Gaussian process. This assumption allows for an accurate representation of the stochastic nature of noise in this analysis.
- $\bar{\mathbf{A}}_t(\varphi_K)$ and $\bar{\mathbf{A}}_r(\theta_K)$ denote the steering matrices of the uniform linear transmit and receive arrays, respectively:

$$\bar{\mathbf{A}}_t(\varphi_K) = \left[\mathbf{a}_t(\varphi_1), \ldots, \mathbf{a}_t(\varphi_K)\right] , \tag{3}$$

$$\bar{\mathbf{A}}_r(\theta_K) = \left[\mathbf{a}_r(\theta_1), \ldots, \mathbf{a}_r(\theta_K)\right] . \tag{4}$$

The steering vectors $\bar{\mathbf{a}}_t(\varphi_i)$ and $\bar{\mathbf{a}}_r(\theta_i)$ are given by:

$$\bar{\mathbf{a}}_t(\varphi_i) = \left[1, e^{-j\frac{2\pi}{\lambda} d \sin(\varphi_i)}, e^{-j\frac{2\pi}{\lambda} 2d \sin(\varphi_i)}, \ldots, e^{-j\frac{2\pi}{\lambda}(M-1) d \sin(\varphi_i)}\right] , \tag{5}$$

$$\bar{\mathbf{a}}_r(\theta_i) = \left[1, e^{-j\frac{2\pi}{\lambda} d \sin(\theta_i)}, e^{-j\frac{2\pi}{\lambda} 2d \sin(\theta_i)}, \ldots, e^{-j\frac{2\pi}{\lambda}(N-1) d \sin(\theta_i)}\right] . \tag{6}$$

S denotes the transmitted baseband-coded waveform matrix in the following way:

$$S = [s_1, \ldots, s_M] . \tag{7}$$

In practical applications, both the transmitter and receiver are affected by mutual coupling. It is typically undesirable because energy that should be radiated outward is instead absorbed by a nearby antenna element. Similarly, energy that one antenna could have captured may be absorbed by a neighboring antenna. Consequently, mutual coupling negatively impacts the efficiency and overall performance of the antenna system. The array of HWD antennas is conceptualized as a multiport network, where the coupling matrix can be directly linked to the generalized impedance matrix of this network.

To compute the mutual coupling matrix $\bar{C}_t$ or $\bar{C}_r$, we account for the interactions among the elements of the matrix, resulting in mutual coupling effects. The array, comprising M (or N) coupled antennas is conventionally depicted as a M (or N) port network, as illustrated in Fig. 2. The mutual coupling matrix $\bar{C}_t$ or $\bar{C}_r$ can be expressed as detailed in [18], [22]–[24]:

$$\bar{C}_t = \left(\bar{Z}_{TA} + \bar{Z}_{TL}\right) \left(\bar{Z}_{Tij} + \bar{Z}_{TL}\bar{I}\right)^{-1} , \tag{8}$$

$$\bar{C}_r = \left(\bar{Z}_{RA} + \bar{Z}_{RL}\right) \left(\bar{Z}_{Rij} + \bar{Z}_{RL}\bar{I}\right)^{-1} , \tag{9}$$

where:

- $\bar{Z}_{TA}$ antenna impedance of isolated antennas in the transmitter,
- $\bar{Z}_{TL}$ terminating load in the transmitter,
- $\bar{Z}_{RA}$ antenna impedance of isolated antennas in the receiver,
- $\bar{Z}_{RL}$ terminating load in the receiver,
- $\bar{Z}_{Tij}$ mutual impedance between the i-th and j-th transmitter elements,
- $\bar{Z}_{Rij}$ mutual impedance between the i-th and j-th receiver elements.

In Eqs. (8)–(9), $\bar{C}_t$ and $\bar{C}_r$ denote the $M \times M$ and $N \times N$ mutual coupling matrices.

$\bar{C}_t$ and $\bar{C}_r$ can be written as:

$$\bar{C}_t = \begin{bmatrix} c_{11} & c_{12} & c_{13} & \ldots & c_{1M} \\ c_{21} & c_{22} & c_{23} & \ldots & c_{2M} \\ \vdots & \vdots & \vdots & \vdots & \vdots \\ \vdots & \vdots & \vdots & \vdots & \vdots \\ c_{M1} & c_{M2} & c_{M3} & \ldots & c_{MM} \end{bmatrix} , \tag{10}$$

$$\bar{C}_r = \begin{bmatrix} c_{11} & c_{12} & c_{13} & \dots & c_{1N} \\ c_{21} & c_{22} & c_{23} & \dots & c_{2N} \\ \vdots & \vdots & \vdots & \vdots & \vdots \\ \vdots & \vdots & \vdots & \vdots & \vdots \\ c_{N1} & c_{N2} & c_{N3} & \dots & c_{NN} \end{bmatrix} . \tag{11}$$

In Eq. (1), it is evident that the coupling matrix influences the signal, leaving the noise unaffected. Once the coupling is characterized, compensating for the mutual coupling becomes a manageable task. Various compensation algorithms can be employed for this purpose, such as the open-circuit voltage method, the S parameter method, the full wave electromagnetic method of moments, the calibration method, and the mutual impedance methods.

Moreover, the coupling values exhibit approximate uniformity along the diagonals, allowing for modeling with a single parameter for each subdiagonal, thus resulting in a coupling matrix of the Toeplitz structure. Leveraging these insights, a compensated coupling model can be formulated as follows [23]:

$$\bar{C}_t = \begin{bmatrix} 1 & c_2 & c_3 & \dots & c_M \\ c_2 & 1 & c_2 & \dots & c_{M-1} \\ c_3 & c_2 & \ddots & \ddots & \vdots \\ \vdots & c_3 & \ddots & 1 & c_2 \\ c_M & c_{M-1} & \dots & c_2 & 1 \end{bmatrix} , \tag{12}$$

$$\bar{C}_r = \begin{bmatrix} 1 & c_2 & c_3 & \dots & c_N \\ c_2 & 1 & c_2 & \dots & c_{N-1} \\ c_3 & c_2 & \ddots & \ddots & \vdots \\ \vdots & c_3 & \ddots & 1 & c_2 \\ c_N & c_{N-1} & \dots & c_2 & 1 \end{bmatrix} . \tag{13}$$

We can put:

$$\mathbf{A}_{ct}(\varphi_i) = \mathbf{C}_t(\varphi_i) \cdot \mathbf{A}_t^T(\varphi_i) , \tag{14}$$

$$\mathbf{A}_{cr}(\theta_i) = \mathbf{C}_r(\theta_i) \cdot \mathbf{A}_r^T(\theta_i) . \tag{15}$$

Therefore, the output of $X(L)$ can be written as:

$$X(L) = \sum_{i=1}^{K} \beta_i(L) \cdot \mathbf{A}_{cr} \cdot \mathbf{A}_{ct} \cdot \mathbf{S}(t) + Z(L) . \tag{16}$$

When $\mathbf{S}^H$ is used as the matched filter matrix, the radar output of the matched filter can be formulated as follows:

$$\begin{aligned} \mathbf{Y}^{(l)} &= \frac{1}{\sqrt{T}} \mathbf{X}^{(l)} \mathbf{S}^H \\ &= \sum_{i=1}^{K} \sqrt{T}\, \beta_i(l)\, \mathbf{A}_{cr} \mathbf{A}_{ct} + \frac{1}{\sqrt{T}} \mathbf{Z}^{(l)} \mathbf{S}^H . \end{aligned} \tag{17}$$

Performing the vectorization operation on Eq. (17), we obtain [19]:

$$\mathbf{y}^{(l)} = \mathrm{vec}\left(\mathbf{Y}^{(l)}\right) . \tag{18}$$

The obtained vector $\mathbf{y}^{(l)}$ can be written as:

$$\mathbf{y}^{(l)} = \mathbf{A}(\varphi_i, \theta_i) \cdot \mathbf{B} + \mathbf{N}^{(l)} , \tag{19}$$

where:

$$\mathbf{N} = \mathrm{vec}\left(\frac{1}{\sqrt{T}} \mathbf{Z}^{(l)} \mathbf{S}^H\right) , \tag{20}$$

and $(\varphi_i^t, \theta_i^r)$ denotes the total manifold matrix with respect to both the array of the transmitter and receiver.

Then:

$$\mathbf{A}(\varphi_i, \theta_i) = \mathbf{A}_{ct}(\varphi_i) \otimes \mathbf{A}_{cr}(\theta_i) . \tag{21}$$

The covariance matrices of the received data y can be written in such a way:

$$\mathbf{C}_{MN} = \mathbf{R}_{yy} = \mathbb{E}\left[\mathbf{y}\mathbf{y}^H\right] , \tag{22}$$

$$\mathbf{C}_{MN} = \mathbf{A}\mathbb{E}\left[\mathbf{B}\mathbf{B}^H\right]\mathbf{A}^H + \mathbb{E}\left[\mathbf{N}\mathbf{N}^H\right] , \tag{23}$$

$$\mathbf{C}_{MN} = \mathbf{A}\mathbf{R}_{BB}\mathbf{A}^H + \sigma_Z^2 \mathbf{I}_{MN} . \tag{24}$$

3. Estimation by the Capon Algorithm

Capon estimation, also known as the minimum-variance distortionless response method, is an advanced signal processing technique used to estimate the parameters of a received signal in a noisy environment disrupted by interference sources.

This estimation aims to minimize the noise power in a given direction, allowing for a more accurate estimation of the parameters of the signal of interest, especially in scenarios with interference sources. This method is widely used in fields such as radar, wireless communications, and sonar processing to improve the resolution and sensitivity of communication systems.

The principle of the Capon algorithm is to find the weighting vector $\mathbf{w}(k)$ that minimizes the total output power of the beamformer while maintaining unity gain in the desired directions. This minimization can be solved using the method of Lagrange multipliers. The beamformer output is provided by [12], [14], [25]:

$$Y_f(t) = \mathbf{w}^H \cdot \mathbf{y}(t) . \tag{25}$$

Once the Y_f is obtained, it is useful to study the spatial covariance matrix of $\mathbf{Y}_f(t)$, denoted as $\mathbf{R}_{Y_f Y_f}$. Ideally, this is defined as the statistical expectation:

$$\mathbf{R}_{Y_f Y_f} = \mathbb{E}\left[\mathbf{Y}_f(t)\mathbf{Y}_f^*(t)\right] = \mathbf{w}^H \cdot \mathbf{C}_{MN} \cdot \mathbf{w} , \tag{26}$$

where, $\mathbf{C}_{MN}$ is the covariance matrix of the input signal vector $\mathbf{y}(t)$. However, since the true expectation $\mathbb{E}[\cdot]$ cannot be computed directly in practice, it is approximated using a time average on the snapshots of the L signal:

$$\widehat{\mathbf{R}}_{Y_f Y_f} = \frac{1}{L} \sum_{t=1}^{L} \mathbf{Y}_f(t)\mathbf{Y}_f^H(t) = \mathbf{w}^H\, \widehat{\mathbf{C}}_{MN}\, \mathbf{w} , \tag{27}$$

where $\widehat{\mathbf{C}}_{MN}$ is the sample covariance matrix of the received signal vector $\mathbf{y}(t)$ estimated over L snapshots.

The Capon method aims to minimize the output power while preserving the signal from the desired direction. The main objective of the Capon algorithm is to suppress interference and noise from other directions, ensuring that the desired signal remains undistorted. This optimization can be formulated as follows.

$$\min_{\mathbf{w}} \left(\mathbf{w}^H \widehat{\mathbf{C}}_{MN} \mathbf{w} \right), \tag{28}$$

subject to the constraint: $\left| w^H \cdot \mathbf{A}(\varphi_i, \theta_i) \right| = 1$.

The solution to this optimization problem yields the Capon weight vector:

$$\mathbf{w} = \frac{\widehat{\mathbf{C}}_{MN}^{-1} \mathbf{A}(\varphi_i, \theta_i)}{\mathbf{A}^H(\varphi_i, \theta_i) \widehat{\mathbf{C}}_{MN}^{-1} \mathbf{A}(\varphi_i, \theta_i)}. \tag{29}$$

Here, $\mathbf{C}_{MN}^{-1}$ represents the inverse covariance matrix of the received data see Eq. (24), which corresponds specifically to the upper triangular matrix $\mathbf{R}$ obtained from the QR decomposition of the matrix $\mathbf{C}_{MN}$.

In this paper, following the approach of [12], the covariance matrix $\mathbf{C}_{MN}^{-1}$ is used in its theoretical form for algorithm development and performance analysis. However, in practical implementations, this matrix must be estimated from measurements, typically using the sample covariance computed from received signal snapshots.

To estimate the direction parameters (φ_i, θ_i), we design a peak-searching function based on the Capon output power spectrum, defined as:

$$P(\varphi, \theta) = \frac{1}{\mathbf{A}^H(\varphi, \theta) \widehat{\mathbf{C}}_{MN}^{-1} \mathbf{A}(\varphi, \theta)}. \tag{30}$$

4. Numerical Results

In this section, the simulation results are presented to elucidate the efficacy of the proposed algorithm. We consider a bistatic MIMO radar system consisting of two uniform linear arrays, comprising M and N HWD antennas. To examine the effect of element separation d on the mutual coupling in a linear array, we simulated the real and imaginary parts of the mutual coupling impedance between two half-wavelength dipoles as a function of their separation, as shown in Fig. 2. As the distance between the elements increases, the magnitude of the mutual coupling impedance decreases and approaches zero.

In the first test, we evaluate the effectiveness and performance of the Capon method in achieving higher resolution for the joint estimation of the direction of departure (DOD) and direction of arrival (DOA) of target signals.

Figure 3 shows the root mean square error (RMSE) of the DOD/DOA estimate versus the signal-to-noise ratio (SNR) for three different uniform linear antenna array configurations: an array without coupling, an array with coupling, and an array with coupling using the compensated algorithm.

We considered four targets with departure angles of $[-30°, -10°, 20°, 60°]$ and arrival angles of $[-40°, -20°, 10°, 50°]$. The system parameters are set to $M = 16$ transmit antennas and $N = 8$ receive antennas,

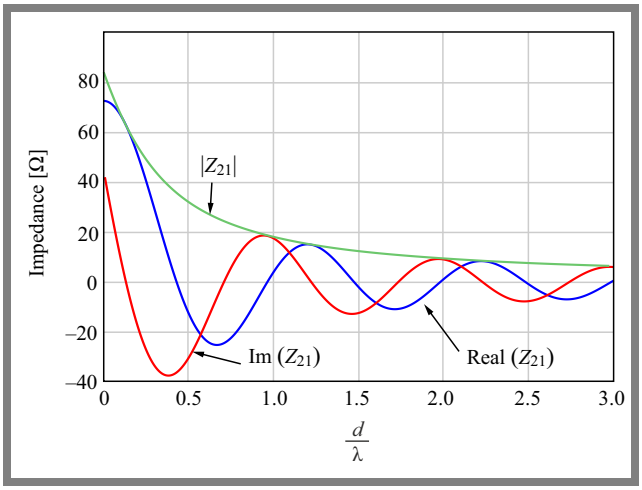

Fig. 2. Coupling impedance versus $\frac{d}{\lambda}$

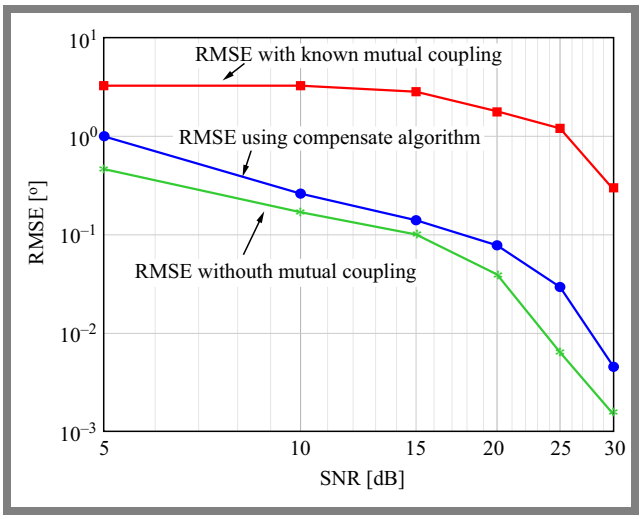

Fig. 3. RMSE versus SNR for DOD $= [-30°, -10°, 20°, 60°]$, DOA $= [-40°, -20°, 10°, 50°]$, $M = 16$, and $N = 8$.

with 250 signal snapshots. Performance is evaluated using the root mean square error (RMSE), computed over 600 Monte Carlo trials, using the following formula [26]:

$$\text{RMSE} = \sqrt{\frac{1}{VK} \sum_{v=1}^{V} \sum_{l=1}^{K} \left[(\hat{\varphi}_{l,v} - \varphi_l)^2 + \left(\hat{\theta}_{l,v} - \theta_l \right)^2 \right]}, \tag{31}$$

where, $\hat{\varphi}_{l,v}$ and $\hat{\theta}_{l,v}$ are the estimated DOD and DOA, respectively, of the K-th target in the V-th Monte Carlo trial. Here, $K = 4$ denotes the total number of targets and $V = 600$ is the number of trials used to average performance.

The results clearly demonstrate that mutual coupling effects cause significant degradation in estimation performance, particularly when the antennas are closely spaced. Moreover, the influence of known mutual coupling on the DOD/DOA estimation is SNR-dependent, with its impact generally decreasing as the SNR increases.

To better understand the behavior of the proposed algorithm, Fig. 4 illustrates the relationship between RMSE and the number of snapshots at a fixed SNR of 25 dB. The number of snapshots varies from 50 to 350. The results clearly show that

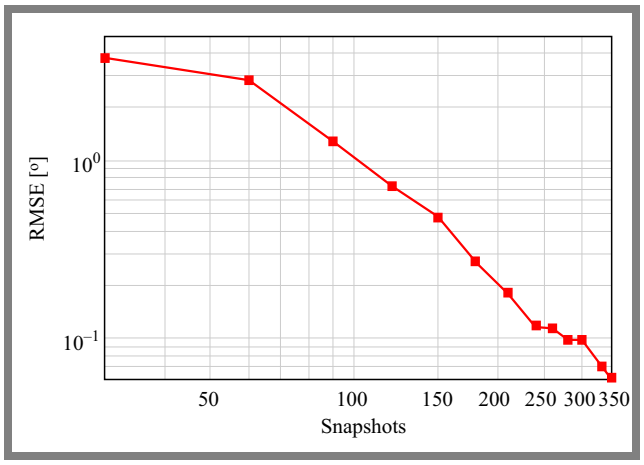

Fig. 4. RMSE versus snapshots with parameters: $M = 16$, $N = 8$, DOD $= [-30°, -10°, 20°, 60°]$, DOA $= [-40°, -20°, 10°, 50°]$, and SNR $= 25$ dB.

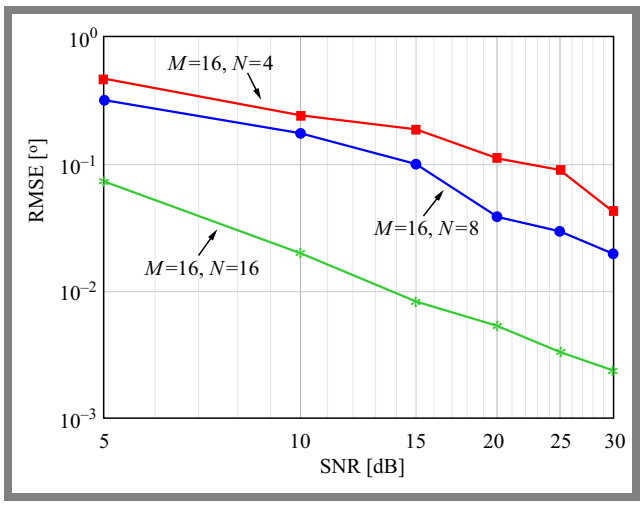

Fig. 5. RMSE versus SNR for different values of N, with $M = 16$, DOD $= [-30°, -10°, 20°, 60°]$, DOA $= [-40°, -20°, 10°, 50°]$, $L = 350$, and $d = \lambda/2$.

the accuracy of the estimation, as indicated by the RMSE, improves consistently with an increasing number of snapshots. This improvement is expected, as a higher number of snapshots enhances the estimation of the covariance matrix and effectively increases the SNR through temporal averaging, leading to more accurate DOD/DOA estimates.

In Fig. 5, the number of transmitting antennas M is fixed, while the number of receiving antennas N is varied. The results indicate that as the number of receiving antennas increases, the RMSE steadily decreases, demonstrating a consistent improvement in the accuracy of the estimation.

In Fig. 6, the number of receiving antennas N is kept constant, while the number of transmitting antennas M is varied. The results indicate that as the number of transmitting antennas increases, the RMSE steadily decreases, highlighting a significant improvement in estimation accuracy. Based on the results presented in Figs. 5 and 6, we observed that increasing the number of transmitting and receiving antennas results in a minimum RMSE, indicating more accurate estimations of the DOA and DOD.

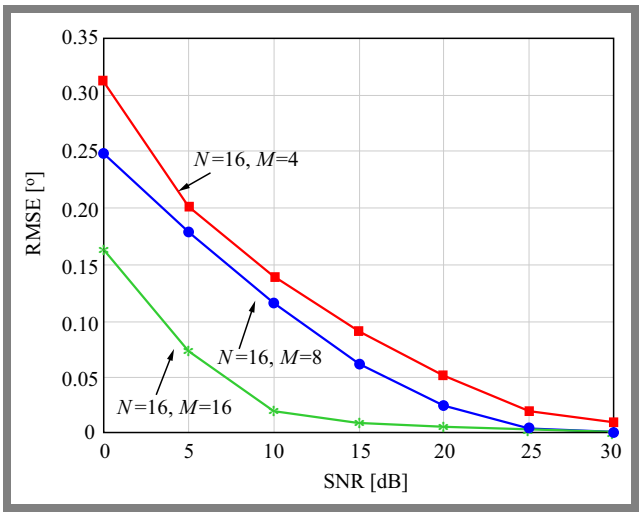

Fig. 6. RMSE versus SNR for different values of M, with $N = 16$, DOD $= [-30°, -10°, 20°, 60°]$, DOA $= [-40°, -20°, 10°, 50°]$, $L = 350$, $d = \lambda/2$, and SNR $= 25$ dB.

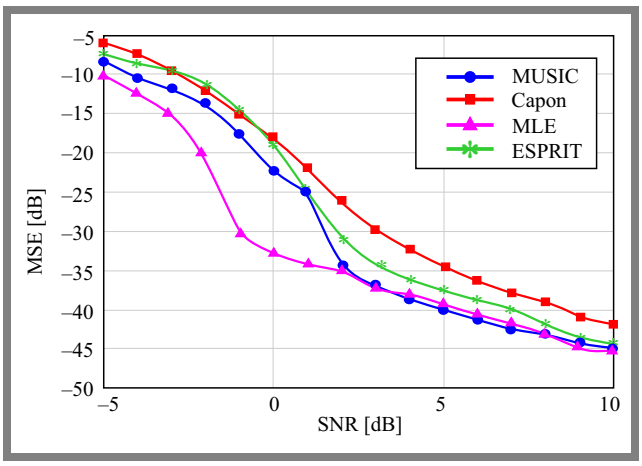

Fig. 7. Mean square error (MSE) versus SNR for DOD.

Figures 7 and 8 present the simulation results for a bistatic MIMO radar system equipped with $M = 5$ transmitting and $N = 5$ receiving antennas, both configured as uniform linear arrays (ULAs) with half-wavelength inter-element spacing. Three target scenarios are evaluated: $(30°, 45°)$, $(-8°, 30°)$, and $(0°, 5°)$, using 100 snapshots and 50 Monte Carlo trials.

Based on the results illustrated in Fig. 7 (DOD) and Fig. 8 (DOA), the mean squared error trends clearly indicate that the accuracy of angle estimation techniques improves as the signal-to-noise ratio increases. The maximum likelihood estimation (MLE) method demonstrates the best overall performance, achieving the lowest MSE.

The ESPRIT algorithm also provides high precision, with performance closely matching that of MLE, especially from 0 dB onward. Although the MUSIC method performs slightly below ESPRIT and MLE, it remains highly effective and exhibits a consistent reduction in MSE as the SNR increases.

In contrast, the Capon method shows comparatively lower performance, particularly under low-SNR conditions, indicating greater sensitivity to noise. However, beyond 5 dB, its MSE decreases significantly, suggesting improved robustness

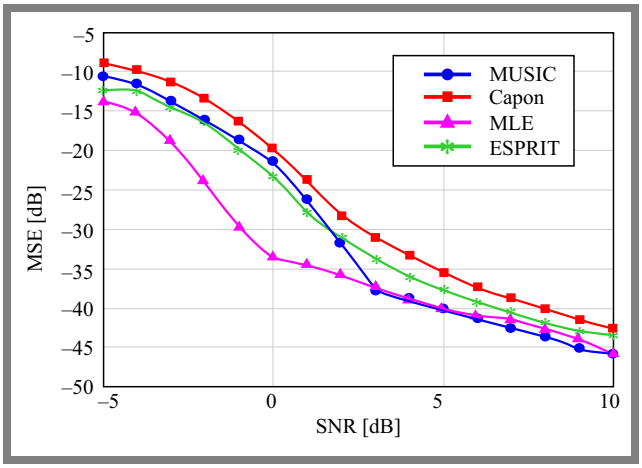

Fig. 8. Mean square error (MSE) versus SNR for DOA.

under moderate noise levels. In summary, MLE offers the highest estimation accuracy, followed by ESPRIT and MUSIC. Although Capon is less precise, it may be preferred in scenarios where reduced computational complexity is a priority [9], [27], [28].

Figure 9 shows the simulation results for signals departing from angles of $[-30°, -15°, 10°, 40°]$, also utilizing 16 antennas, an SNR of approximately 25 dB, and 350 snapshots. The element spacing in the array remains at $\lambda/2$. Here, we again observe four distinct peaks that align with the desired angles of departure.

Figure 10 presents the simulation results for signals coming from angles of $[-20°, -10°, 30°, 60°]$ using 16 antennas, an SNR of approximately 25 dB, and 350 snapshots. The spacing between the elements of the array is set to $\lambda/2$. In this case, we observe four distinct peaks corresponding to the desired angles of arrival. Furthermore, it is evident that the departure angles (DODs) and arrival angles (DOAs) can be clearly distinguished.

Figures 9 and 10 reveal that the spatial spectrum reaches its maxima at angles corresponding to DOD values of $-30°$, $-15.004°$, $9.992°$, and $40.001°$, and DOA values of $-19.995°$, $-9.999°$, $30°$, and $60°$. The precision of these estimates indicates that the angular search was performed on a finely spaced grid, probably with a step size of $0.01°$.

Figure 11 shows the estimation results for four targets, the SNR is set at 25 dB, with 350 snapshots. The results demonstrate that the DODs and DOAs are clearly observable and are automatically paired. In the following simulation, 500 Monte Carlo iterations are performed for the bistatic MIMO radar. We assume the presence of four non-coherent targets located at angles $(\varphi_1, \theta_1) = (-30°, -20°)$, $(\varphi_2, \theta_2) = (-15°, -10°)$, $(\varphi_3, \theta_3) = (10°, 30°)$, and $(\varphi_4, \theta_4) = (40°, 60°)$, respectively. It can be shown that the transmit angles (DODs) and the receive angles (DOAs) can be clearly observed.

5. Conclusions

In this paper, we examine the estimation of the direction of departure (DOD) and direction of arrival (DOA) for bistatic MIMO radar systems in the presence of known mutual coupling. Our study is grounded in fundamental electromagnetic principles and employs the Capon algorithm to achieve accurate signal estimation. Through computer simulations, we analyze the influence of various parameters on the performance of the Capon algorithm, focusing on its ability to efficiently and accurately resolve incoming signals.

Simulation results demonstrate that the DOD/DOA estimation performance improves with an increased number of array ele-

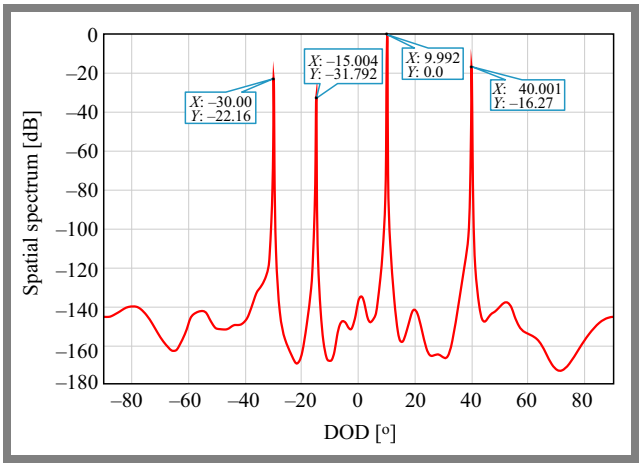

Fig. 9. Spatial spectrum versus DODs with $M_1 = N = 16$, DOD $= [-30°, -15°, 10°, 40°]$, DOA $= [-20°, -10°, 30°, 60°]$, $L = 350$, $d = \lambda/2$, and SNR $= 25$ dB.

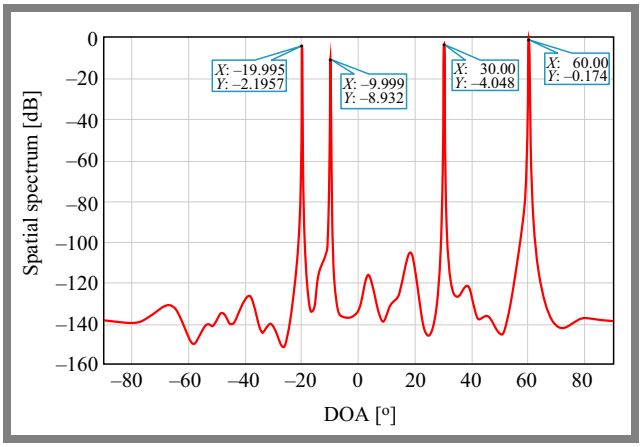

Fig. 10. Spatial spectrum versus DOAs with $M_1 = N = 16$, DOD $= [-30°, -15°, 10°, 40°]$, DOA $= [-20°, -10°, 30°, 60°]$, $L = 350$, $d = \lambda/2$, and SNR $= 25$ dB.

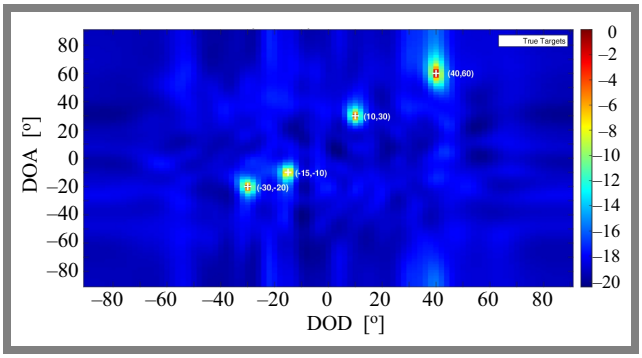

Fig. 11. Angle estimation of the proposed algorithm for four targets.

ments, a higher number of signal snapshots, and array spacing is $\lambda/2$. These enhancements result in sharper spectral peaks and reduced angular detection errors, highlighting the effectiveness of the Capon algorithm in estimating the DOD/DOA of incoming signals. However, despite these improvements, the known mutual coupling among HWD antennas introduces significant distortions to the output signal. This distortion negatively impacts the joint DOD/DOA estimation performance for multiple targets in bistatic MIMO radar systems using the Capon algorithm. To address these challenges, we recommend employing a compensation algorithm to mitigate the adverse effects of mutual coupling.

References

[1] J. Li and P. Stoica, "MIMO Radar with Colocated Antennas", *IEEE Signal Processing Magazine*, vol. 24, pp. 106–114, 2007 (https://doi.org/10.1109/MSP.2007.904812).

[2] B. Liao, "Fast Angle Estimation for MIMO Radar with Nonorthogonal Waveforms", *IEEE Transactions on Aerospace and Electronic Systems*, vol. 54, pp. 2091–2096, 2018 (https://doi.org/10.1109/TAES.2018.2847958).

[3] A.M. Haimovich, R.S. Blum, and L.J. Cimini, "MIMO Radar with Widely Separated Antennas", *IEEE Signal Processing Magazine*, vol. 25, pp. 116–129, 2008 (https://doi.org/10.1109/MSP.2008.4408448).

[4] P. Woodward, *Probability and Information Theory with Applications to Radar*, 3rd ed., Norwood, MA: Artech House, 128 p., 1980 (ISBN: 9780890061039).

[5] J. Chen, H. Gu, and W. Su, "A New Method for Joint DOD and DOA Estimation in Bistatic MIMO Radar", *Signal Processing*, vol. 90, pp. 714–718, 2010 (https://doi.org/10.1016/j.sigpro.2009.08.003).

[6] T.-Q. Xia, "Joint Diagonalization Based DOD and DOA Estimation for Bistatic MIMO Radar", *Signal Processing*, vol. 108, pp. 159–166, 2015 (https://doi.org/10.1016/j.sigpro.2014.09.010).

[7] M. Jin, G. Liao, and J. Li, "Joint DoD and DoA Estimation for Bistatic MIMO Radar", *Signal Processing*, vol. 89, pp. 244–251, 2009 (https://doi.org/10.1016/j.sigpro.2008.08.003).

[8] X. Zhang, C. Chen, and J. Li, "Angle Estimation Using Quaternion-ESPRIT in Bistatic MIMO-Radar", *Wireless Personal Communication*, vol. 69, pp. 551–560, 2013 (https://doi.org/10.1007/s11277-012-0589-3).

[9] C. Duofang, C. Baixiao, and Q. Guodong, "Angle Estimation Using ESPRIT in MIMO Radar", *Electronics Letters*, vol. 44, pp. 770–771, 2008 (https://doi.org/10.1049/el:20080276).

[10] M.L. Bencheikh and Y. Wang, "Joint DOD-DOA Estimation Using Combined ESPRIT-MUSIC Approach in MIMO Radar", *Electronics Letters*, vol. 46, pp. 1081–1083, 2010 (https://doi.org/10.1049/el.2010.1195).

[11] G. Zheng, B. Chen, and M. Yang, "Unitary ESPRIT Algorithm for Bistatic MIMO Radar", *Electronics Letters*, vol. 48, pp. 179–181, 2012 (https://doi.org/10.1049/el.2011.3657).

[12] X. Zhang and D. Xu, "Angle Estimation in Bistatic MIMO Radar Using Improved Reduced Dimension Capon Algorithm", *Journal of Systems Engineering and Electronics*, vol. 24, pp. 84–89, 2013 (https://doi.org/10.1109/JSEE.2013.00011).

[13] S.-W. Chen, C.-L. Meng, and A.-C. Chang, "DOA and DOD Estimation Based on Double 1-D Root-MVDR Estimators for Bistatic MIMO Radars", *Wireless Personal Communication*, vol. 86, pp. 1321–1332, 2016 (https://doi.org/10.1007/s11277-015-2991-0).

[14] R. Sanudin *et al.*, "Capon-like DOA Estimation Algorithm for Directional Antenna Arrays", *2011 Loughborough Antennas & Propagation Conference*, Loughborough, UK, 2011 (https://doi.org/10.1109/LAPC.2011.6114042).

[15] Z. Zhidong, Z. Jianyun, and N. Chaoyan, "Angle Estimation of Bistatic MIMO Radar in the Presence of Unknown Mutual Coupling", *2011 IEEE CIE International Conference on Radar*, Chengdu, China, 2011 (https://doi.org/10.1109/CIE-Radar.2011.6159474).

[16] C. Zhang, H. Huang, and B. Liao, "Direction Finding in MIMO Radar With Unknown Mutual Coupling", *IEEE Access*, vol. 5, pp. 4439–4447, 2017 (https://doi.org/10.1109/ACCESS.2017.2684465).

[17] B.T. Arnold and M.A. Jensen, "The Effect of Antenna Mutual Coupling in a MIMO Radar System", *IEEE Transactions on Antennas and Propagation*, vol. 67, pp. 1410–1416, 2017 (https://doi.org/10.1109/TAP.2018.2888702).

[18] P. Chen, Z. Cao, Z. Chen, and C. Yu, "Sparse DOD/DOA Estimation in a Bistatic MIMO Radar with Mutual Coupling Effect", *Electronics*, vol. 7, art. no. 341, 2018 (https://doi.org/10.3390/electronics7110341).

[19] J. Hu, E. Baidoo, and Z. Bao, "High-resolution Angle Estimation Method in Partly Calibrated Subarray-based Bistatic Multiple-input Multiple-output Radar with Unknown Non-uniform Noise", *IET Radar, Sonar and Navigation*, vol. 16, pp. 704–719, 2021 (https://doi.org/10.1049/rsn2.12214).

[20] Y. Guo, Y. Zhang, N. Tong, and J. Gong, "Angle Estimation and Self-calibration Method for Bistatic MIMO Radar with Transmit and Receive Array Errors", *Circuits, Systems, and Signal Processing*, vol. 36, pp. 1514–1534, 2017 (https://doi.org/10.1007/s00034-016-0365-9).

[21] F. Dong, C. Shen, K. Zhang, and H. Wang, "Real-valued Sparse DOA Estimation for MIMO Array System under Unknown NonUniform Noise", *IEEE Access*, vol. 6, pp. 52218–52226, 2018 (https://doi.org/10.1109/ACCESS.2018.2870257).

[22] N. Boughaba, O. Barkat, and C. Chettah, "Adaptive Beamforming Algorithm Based on MVDR for Smart Linear Dipole Array with Known Mutual Coupling", *Progress In Electromagnetics Research C*, vol. 124, pp. 125–134, 2022 (https://doi.org/10.2528/PIERC22080103).

[23] M. Bensalem and O. Barkat, "DOA Estimation of Linear Dipole Array with Known Mutual Coupling Based on ESPRIT and MUSIC", *Radio Science*, vol. 57, pp. 1–15, 2022 (https://doi.org/10.1029/2021RS007294).

[24] N. Boughaba and O. Barkat, "LMS and RLS Beamforming Algorithms Based Linear Antenna Array with Known Mutual Coupling", *Journal of Electromagnetic Waves and Applications*, vol. 37, pp. 1449–1462, 2024 (https://doi.org/10.1080/09205071.2023.2251979).

[25] X. Zhang and D. Xu, "Angle Estimation in MIMO Radar Using Reduced-dimension Capon", *Electronics Letters*, vol. 46, pp. 860–861, 2010 (https://doi.org/10.1049/el.2010.0346).

[26] H. Chen *et al.*, "Joint DOD and DOA Estimation for Bistatic MIMO Radar without Eigenvalue Decomposition", *Progress In Electromagnetics Research Letters*, vol. 80, pp. 67–74, 2018 (https://doi.org/10.2528/PIERL18100106).

[27] C. Jinli, G. Hong, and S. Weimin, "Angle Estimation Using ESPRIT without Pairing in MIMO Radar", *Electronics Letters*, vol. 44, pp. 1422–1423, 2008 (https://doi.org/10.1049/el:20089089).

[28] B. Tang, J. Tang, Y. Zhang, and Z. Zheng, "Maximum Likelihood Estimation of DOD and DOA for Bistatic MIMO Radar", *Signal Processing*, vol. 93, pp. 1349–1357, 2013 (https://doi.org/10.1016/j.sigpro.2012.11.011).

Ouarda Barkat, Professor
Department of Electronics
https://orcid.org/0000-0001-6784-8338
E-mail: barkat.ouarda@umc.edu.dz
University of Frères Mentouri – Constantine 1, Constantine, Algeria
https://www.umc.edu.dz